The Journal of Chemical Physics

RESEARCH ARTICLE | FEBRUARY 24 2026

Ultrafast radiation chemistry of glycine in aqueous solution

Special Collection: Simulation of excited state dynamics in molecular and condensed-matter systems

Mathilde Goullieux ; Anthony Ferté ; Ana Martinez Gutierrez ; Ludger Inhester ; Robin Santra

J. Chem. Phys. 164, 084504 (2026)
https://doi.org/10.1063/5.0316290

The Journal of Chemical Physics ARTICLE pubs.aip.org/aip/jcp

Ultrafast radiation chemistry of glycine in aqueous solution

Cite as: J. Chem. Phys. 164, 084504 (2026); doi: 10.1063/5.0316290
Submitted: 11 December 2025 • Accepted: 10 February 2026 •
Published Online: 24 February 2026

Mathilde Goullieux,[1,a] Anthony Ferté,[1] Ana Martinez Gutierrez,[2] Ludger Inhester,[1,3] and Robin Santra[1,3,4,b]

AFFILIATIONS

[1] Center for Free-Electron Laser Science CFEL, Deutsches Elektronen-Synchrotron DESY, Notkestr. 85, 22607 Hamburg, Germany
[2] Instituto de Ciencia de Materiales de Madrid Consejo Superior de Investigaciones Científicas (ICMM-CSIC), Calle Sor Juana Inés de la Cruz 3, Campus de Cantoblanco, 28049 Madrid, Spain
[3] The Hamburg Centre for Ultrafast Imaging, Luruper Chaussee 149, 22761 Hamburg, Germany
[4] Department of Physics, University of Hamburg, Notkestr. 9-11, 22607 Hamburg, Germany

Note: This paper is part of the Special Topic, Simulation of Excited State Dynamics in Molecular and Condensed-Matter Systems.
[a] **Author to whom correspondence should be addressed:** mathilde.goullieux@desy.de
[b] **Electronic mail:** robin.santra@cfel.de

ABSTRACT

Investigating the ultrafast dynamics of primary biological compounds is crucial for gaining insights into radiation damage. We computationally investigate the ionization-induced dynamics of glycine in an aqueous solution. By employing fewest-switches-surface hopping simulations, we specifically address ionization in different orbital levels of the glycine molecule as well as in water molecules in its solvation shell. Upon ionization, glycine undergoes rapid fragmentation on the C_α–C bond, resulting in the formation of CO_2 and the methylamine ($^+H_3NH_2C\cdot$) radical. Our analysis shows that the solvation shell has little effect on the fragmentation dynamics. When ionized in water, or a deeper valence orbital of glycine, the system first relaxes to the ground state, involving the transfer of the valence hole between water and glycine. The associated redox reaction exemplifies the oxidizing power of $H_2O^{\cdot+}$.

I. INTRODUCTION

Amino acids (AAs) are the fundamental building blocks of living organisms and play a crucial role in all biological processes. Composed of an amine and a carboxyl group, they assemble through peptide bonds to form essential biomolecules, such as proteins.

Various studies have reported the presence of prebiotic molecules and simple AAs, such as glycine, in meteorites, demonstrating that they can be synthesized in outer space.[1–5] Moreover, AA-formation via the ionization of ammonium moieties has been observed *in vitro*,[6,7] suggesting that radiation plays an important role in the evolution of chemical complexity in outer space. However, radiation can also be destructive,[8,9] so understanding the impact of radiation on AAs[10] is crucial for our understanding of abiogenesis. Furthermore, investigating the ionization-induced dynamics of AAs is the foundation for enlightening the impact of radiation on living cells and proteins. This topic is of great importance in the contexts of space travel[11–13] and cancer therapy.[14] Because all living organisms contain a large amount of water, it is particularly important to study the ionization-induced dynamics in aqueous solution, since water plays a central role in solvated-radical processes.[15] At physiological pH (7.4), amino acids exist predominantly in their zwitterionic form in water, whereas in the gas phase (vacuum), they preferentially adopt their neutral form. This structural interconversion is mostly driven by hydrogen bonds (H-bonds).[16–18]

Being the smallest AA, glycine ($C_2H_5NO_2$) has often been used as a model biomolecule for studying radiation-induced damage in vacuum with various types of spectroscopy. The photofragmentation of isolated glycine upon ionization was studied using ultraviolet (UV),[19–22] soft x-ray absorption,[23,24] or ion-induced ionization with mass spectroscopy.[25] In liquid water, glycine was irradiated with MeV ions, and the resulting fragmentation was probed by

secondary-ion mass spectrometry.[26] In ice, glycine–water samples were probed using near-edge x-ray absorption fine structure spectroscopy.[9] These experimental studies have been supported by computational simulations of the dynamics to unravel the influence of structural and electronic changes on spectral features.[9,27,28] All of them have concluded that the fragmentation of the C_α–C bond is the most dominant reaction pathway.[19,23,25–28] So far, most studies focus on glycine in vacuum, and to our knowledge, no theoretical methods have been applied to follow the evolution of ionized and electronically excited zwitterionic glycine in an explicit aqueous environment. In this work, we aim to contribute to the understanding of this unresolved question and investigate the ionization-triggered dynamics of glycine in water.

High-energy radiation can generally induce the population of highly excited ionic states. The electronic relaxation via internal conversion may involve a large number of different potential energy surfaces (PESs).[29] This represents a challenge for modeling the ultrafast reaction dynamics. Moreover, the presence of water as explicit solvent molecules implies additional PESs, increasing the complexity of the problem compared to the situation of an isolated molecule. Over the years, our group has developed a reasonably accurate yet affordable approach, coupling the fewest-switches-surface-hopping (FSSH) method[30] with PESs provided by Koopmans' theorem. This method, previously used to study organic photovoltaics,[31,32] water,[33,34] and urea,[35] gives insights into the dynamics triggered by ionization that can be used for the interpretation of time-dependent spectra. In the present study, we extend its application to the intricate system of interest—hydrated glycine. Using the FSSH method in an embedded quantum mechanics/molecular mechanics (QM/MM) setup, we present here a computational study of the dynamics of aqueous glycine triggered by the ionization of one of the valence electrons, either from glycine or from a water molecule in its solvation shell.

In this study, we specifically address how the dynamics are altered when initial ionization takes place from different orbital energy levels. We report that within about 100 fs, an electronic valence hole can travel through the solute and adjacent water molecules before glycine breaks apart into a carbon dioxide (CO_2) and a methylamine ($^+H_3NH_2C\cdot$) carbocation. The influence of the solvation shell on the fragmentation is also briefly discussed.

In Sec. II, we describe the computational methods. Results are presented in Sec. III, and in Sec. IV, we draw our final conclusions.

II. METHODS

A. Structure preparation and equilibration

The structure of glycine was taken from the protein data bank[36] in sdf file format. Open Babel[37,38] was used to convert the structure in the pdb file format and to protonate the system at pH 7.4 to match biological conditions. At this pH value, glycine is zwitterionic,[18] as depicted at the center of its pKa reaction scheme in Fig. 1. In vacuum, glycine is in its neutral form, $NH_2CH_2CO_2H$; however, in water, the zwitterion is energetically more favored than the neutral form.[39] Therefore, the present study focuses on this specific protonation state of the molecule, which is predominant in neutral pH water conditions.[18,40]

The zwitterion was solvated with GROMACS,[41] using a cubic box of 30 Å box length, to ensure a sufficiently extended water

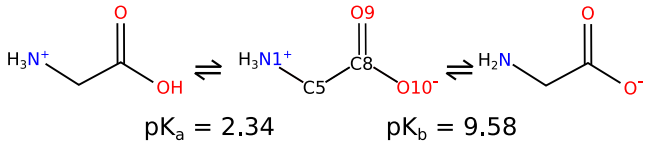

FIG. 1. Protonation states of glycine in water. Atom names are specified for the zwitterionic form. The hydrogen atoms on C5 are omitted.

environment. The system was subsequently equilibrated with force field (FF)-based molecular dynamics (MD) simulations with GROMACS, as described below. First, a short energy minimization was performed to ensure removal of clashes and nonphysical geometries upon addition of water. Then, an NVT MD simulation of 100 ps with a Berendsen thermostat[42] at 300 K was conducted to stabilize the system at room temperature. Two different coupling groups were used for glycine and water molecules, since the solute tends to equilibrate more slowly than water. Finally, the system was equilibrated at 1 bar via a 100 ps NPT simulation.

In the whole study, the same FF parameters were used for all simulations (equilibration, sampling, and ionization), in particular, the CHARMM 27 FF[43–45] for glycine, in combination with the TIP3P water model.[46,47] The CHARMM 27 FF includes all necessary features for treating amino acids in their zwitterionic form, in combination with the TIP3P water model.[45] Periodic boundary conditions (PBCs) were systematically used in all simulations using GROMACS.

B. Sampling thermal fluctuations

Thermal fluctuations play a crucial role in solvated systems, arising primarily from the dynamic motion of water molecules. From the equilibrated MD simulations, FF-based production runs were propagated for 5 ns, with a time step of 2 fs, to sample an ensemble of structures with various geometries. Radial distribution functions and cumulative coordination numbers are compared with the literature data[48–52] in Sec. S1 of the supplementary material.

Then, structural snapshots were collected at different time steps of these FF-based MD-simulation results. The structures were collected every 80 ps between 1 and 5 ns (i.e., a duration of 4 ns), giving a total of 51 evenly spaced snapshots. These were further individually equilibrated with *ab initio* MD (AIMD). The AIMD was performed with the GROMACS QM/MM interface, coupled with the XMOLECULE toolkit[33,53–55] as the QM engine, and employing the restricted Hartree–Fock method with the 6-31G* basis set[56,57] for the electronic structure calculations. Each AIMD simulation was propagated for 1 ps with a time step of 1 fs. This step specifically accounts for the equilibration of hydrogen positions that were constrained in the earlier FF-based MD simulations but are unconstrained in the QM region. The equilibration of these AIMD simulations is further discussed in Sec. S2 of the supplementary material. The division of the system into QM and MM regions is described below.

C. QM/MM scheme

For the AIMD equilibration, the same simulation box of 30 Å was selected. The system was centered on the center of mass of

glycine, and the 20 water molecules closest to the origin were placed in the QM region, the remaining water being treated with classical point charges.

For the ionized-state simulation, the same method as described in Ref. 34 was followed. Out of the QM/MM-post-processed simulation box, a sphere of diameter 30 Å was cut out around the center of mass of glycine (taking into account the PBC). A somewhat smaller QM region was used, consisting of glycine and water molecules composing its first solvation shell.

The size of the QM region is a key factor for the observation of water–glycine interactions. We chose to incorporate ten surrounding water molecules into the QM region. Based on our analysis of the cumulative distribution numbers described in Sec. S1 of the supplementary material, this covers the first solvation shell.

To ensure a proper representation of the first solvation shell around glycine, a bubble scheme was used to decide which water molecule to incorporate into the QM region. A water molecule is included in the QM region if—in order of priority—any of its atoms satisfies one of the following criteria:

- within a distance of 2.5 Å from the *cis*-oxygen atom (O9),
- within a distance of 2.5 Å from the *trans*-oxygen atom (O10), or
- within a distance of 3.5 Å from the nitrogen (N1).

The threshold values correspond to the extension of the first solvation shell on the N and O atoms of the glycine zwitterion.[52] Then, the next closest water molecules to the center of mass of glycine were included—if needed—to reach a total of ten water molecules in the QM region. The remaining solvent was used for the MM region.

We employed electrostatic embedding, where the water molecules in the MM region were represented as smeared-out charges in the electronic-structure calculation of the QM region. The smeared-out charges were described via Gaussian functions, with the integrated charge being the charge defined by the FF and a standard deviation given by the covalent radius of the respective atom (0.66 Å for oxygen and 0.31 Å for hydrogen).[58]

D. Nonadiabatic dynamics

The dynamics following ionization were propagated for at least 100 fs, with a time step of 0.2 fs for the propagation of the molecular geometry.

Upon ionization, the dynamics involve relaxation of the electronic state via nonadiabatic coupling. If a highly excited electronic state is considered, relaxation to the ground state (GS) might involve a large number of PESs. In our approach, these non-Born–Oppenheimer effects are modeled using the FSSH from Tully.[30]

The electronic-structure calculations were performed using the XMOLECULE toolkit,[33,53–55] describing ionization with Koopmans' theorem and providing energies for all hole states. The corresponding gradients and nonadiabatic coupling coefficients were computed on the fly via solving the coupled-perturbed Hartree–Fock equations. All states that can be generated by having a hole in any valence orbital are taken into account for the simulations. Accordingly, the surface-hopping dynamics involved 55 states.

The analysis of structural variations (bonds, angles, and dihedral angles) in the system over time was performed using the MDAnalysis Python package.[59,60] The same package was used to analyze the H-bonds in the system. For defining the H-bonds, we used the default geometric criteria of the package, as used in a former study from our group,[61] namely,

- donor–hydrogen distance below 2.5 Å,
- donor–acceptor distance below 3.5 Å, and
- donor–hydrogen–acceptor angle above 140°.

III. RESULTS

A. Orbital characterization and initial ionization conditions (ICs)

The glycine zwitterion ($^{+}NH_3CH_2CO_2^{-}$) belongs to the C_s symmetry point group and has two irreducible representations, A′ and A″. Glycine has a total of 40 electrons, and its electronic GS corresponds to a closed-shell configuration with 20 doubly occupied molecular orbitals (MOs). Among these, five are core orbitals, whereas the remaining 15 are valence orbitals—11 of A′ symmetry and four of A″ symmetry.[62] Upon addition of water, the QM region (the glycine molecule and ten surrounding water molecules) contains a total of 70 occupied orbitals. The solvation influences the energy and shape of the MOs.[63] Moreover, the presence of the water molecules leads to mixing of some of the glycine and water orbitals. Nevertheless, most of the MOs can be assigned symmetry labels corresponding to glycine and water, respectively. Depending on whether the MO is mostly located on glycine or on water, we employ the "gly-" and "wat-" prefixes, followed by the corresponding orbital label. Considerable mixing between water and glycine is indicated by the label "gly/wat."

Figure 2(a) shows a histogram of the MO energies, using data from the 51 reference geometries. The classification of the MOs was based on electronic population analysis and visual inspection of their shape. A threshold of 0.7 was used to assign whether the MO belongs to water or glycine. As one can see, the three highest occupied MOs of the system—HOMO, HOMO-1, and HOMO-2—belong to the glycine with the major orbital shapes of gly-16-a′, gly-4a″, and gly-15a′, respectively. Their energies overlap so that they appear as a single group that is separated from other orbital classes. We observe that the assignment of the orbital character (gly-16-a′, gly-4a″, and gly-15a′) to the relative energetic position (HOMO, HOMO-1, and HOMO-2) is swapped for some of the sampled configurations. The assignment displayed in Fig. 2(b) corresponds to a typical sampled configuration.

The HOMO-4 to HOMO-40 cover a continuous energy range from binding energies of 13–21 eV. In this energy range are the three outermost MOs of water, wat-1b$_2$, wat-3a$_1$, and wat-1b$_1$. The more strongly bound orbital HOMO-41 (gly-9a′) has a binding energy of about 26 eV, well separated from the other valence orbitals of glycine and water. At the same time, its binding energy is also separated from the ones of inner-valence MOs (below −33 eV, not shown). Selected examples of glycine orbitals are depicted in Fig. 2(b). In particular, one can see that the HOMO, HOMO-1, and HOMO-2 are mostly located on the oxygen atoms of glycine. Typical examples for classes of water molecules are depicted in Fig. 2(c).

To study the ionization-induced dynamics of glycine in water, we consider initial valence holes in selected groups of valence

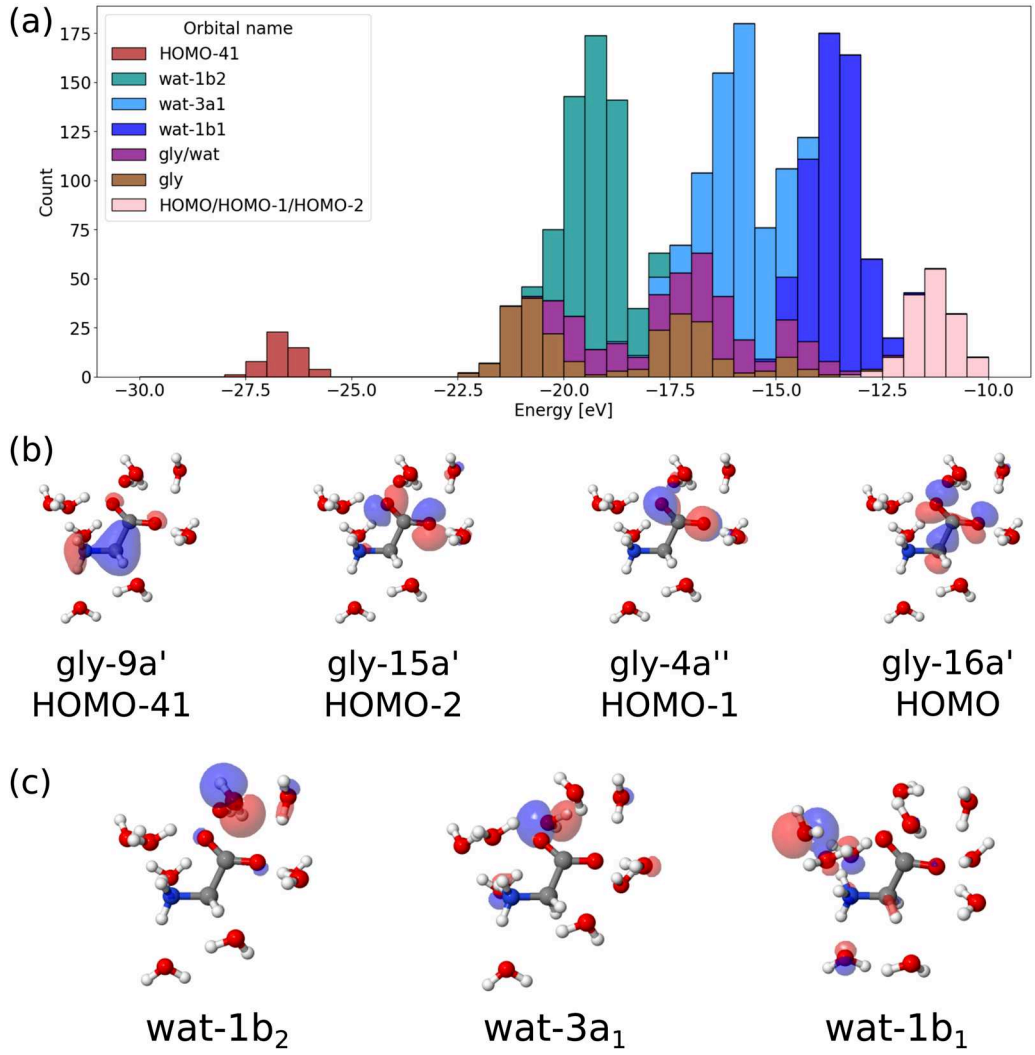

FIG. 2. (a) Histogram of orbital energies for the considered ensemble (QM regions). For the classification into different orbital groups, see the text. (b) Glycine MO representation in the solvated system. (c) Water MO representation in the solvated system. MOs are displayed from JMol,[64] with an isosurface threshold ("`MO cutoff`") of 0.05.

orbitals. In the first scenario (scenario A), we consider valence holes in the group of the three highest occupied orbitals, HOMO, HOMO-1, and HOMO-2. To address the case when the ionization occurs on a water molecule next to the glycine, we create an initial hole in one of the MOs in the water solvation shell (scenario B). As a third scenario (scenario C), we address initial ionization in the deeper bound HOMO-41.

B. Scenario A: Ionization of the glycine in the HOMO, HOMO-1, and HOMO-2

For each of the 51 initial geometries, we consider ionization in each of the HOMO, HOMO-1, and HOMO-2. The 51 initial structures thus result in an ensemble of 153 trajectories. In Fig. 3, we show the fraction of trajectories with an active state in the three different states. By construction, the initial fraction is 1/3, but since the three MOs are close in energy, rapid electronic relaxation to the GS (i.e., the state with the hole in the HOMO) occurs. 90% of the trajectories reach the GS within the first 25 fs after ionization. After 100 fs, only five trajectories (3%) remain in the HOMO-1–hole state, suggesting that a longer simulation time may be required for them to reach the GS.

We observe in a number of trajectories that the ionized glycine molecule dissociates along its C5–C8 bond into a CO_2 fragment and an $^{+}NH_3CH_2$ fragment. The green dashed-dotted line in Fig. 3 shows the fraction of trajectories where the molecule has fragmented (the C5–C8 distance is larger than 3.0 Å). Remarkably, this fraction suddenly increases at about 35 fs and reaches, for some time, a plateau of about 1/3. This increase almost exclusively relates to those trajectories that have an initial hole in MOs with a character of type

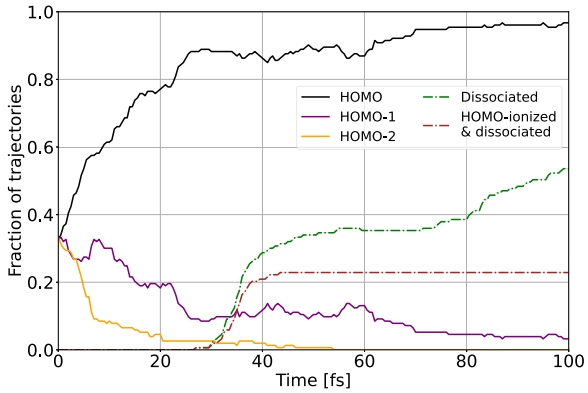

FIG. 3. Fraction of the 153 trajectories with an active state with a valence hole in the HOMO (black), HOMO-1 (purple), and HOMO-2 (orange) as a function of time (solid lines); fraction of all trajectories in which glycine dissociated (green, dashed-dotted line); and fraction of trajectories that started with a HOMO hole and that have dissociated (brown, dashed-dotted line).

gly-16a′. These correspond to 68% of the ones that have an initial hole in the HOMO (brown, dashed-dotted line). In these trajectories, the bond immediately starts elongating so that the molecule is fully dissociated after 40 fs. A further increase can be seen at about 80 fs. This behavior can be explained by the fact that glycine dissociation occurs only in the GS. Trajectories starting with a hole in the HOMO-1 and HOMO-2, therefore, require additional time for the electronic relaxation before they undergo dissociation. Inspection of the data confirmed that all dissociated trajectories are in the GS, while none of the ones being in an excited state have dissociated yet. The finding that the HOMO vacancy triggers bond dissociation can be understood from the orbital pictures in Fig. 2(b). As can be seen, the HOMO-1 and HOMO-2 are localized on the CO_2 moiety, whereas the HOMO spreads also over the C5–C8 bond, indicating its decisive role in the formation of the bond. Accordingly, removing an electron in this orbital weakens this particular bond.

Overall, electronic relaxation occurs first, and subsequently, the bond dissociation is initiated. The fact that dissociation occurs rather coherently for the ensemble of trajectories starting in the HOMO-hole state (68% of these trajectories suddenly show dissociation around 40 fs) suggests that for the remaining ones, the electronic relaxation is the rate-determining step.

C. Internal coordinates upon glycine fragmentation

To further inspect the fragmentation of glycine into $^{+}NH_3CH_2$ and CO_2, we focus now only on those 82 trajectories that show dissociation in the ensemble considered in Fig. 3. We identified the internal coordinates in the glycine molecule that exhibit the strongest changes along the fragmentation. These internal coordinates and the glycine heavy-atom labels are depicted in Fig. 4(a) for a typical initial structure and discussed in Figs. 4(b)–4(e).

Figure 4(b) depicts the evolution of the distribution of interatomic distances between C5 and C8, i.e., the bond along which the molecule fragments. As can be seen, the distance steadily increases as a function of time. The bond distances in the CO_2 moiety are shown in Fig. 4(c). Along with the dissociation, they decrease and eventually reach a value close to 1.16 Å, which is characteristic of CO_2.[65]

Figure 4(d) shows the evolution of two internal angles in the glycine molecule. The θ(O9–C8–O10) angle increases from 130° to 165°, i.e., approaching the equilibrium angle of CO_2 (180°[65]). The remaining nonlinearity may be explained by the presence of H-bonds formed between CO_2 and water. The δ(N1–C5–H6–H7) dihedral angle is defined between the N1 atom and the plane composed of the C5, H6, and H7 atoms, which is represented by the black line in Fig. 4(a). It evolves from a nearly tetrahedral conformation (115°) to a nearly planar (160°) conformation, as reported for the $^{+}H_3NH_2C\cdot$ radical.[66]

In Fig. 4(e), we show the atomically resolved population of the valence hole in the ensemble of dissociating trajectories as a function of time. Since all electrons are paired except the one in the valence-hole orbital, the unpaired spin is entirely associated with the valence hole. Consequently, the atomic valence-hole populations directly reflect the spatial distribution of the spin density and reveal the location of the radical center. The hole population is initially spread over carbon C5 (fraction of 0.14), the two glycine oxygens O9 and O10 (0.40 each), and the N1 atom (0.06). As the dissociation progresses, the valence hole moves almost entirely to the atom C5 (fraction = 0.95), confirming the formation of neutral CO_2 and $^{+}H_3NH_2C\cdot$.

The internal movements of glycine occur simultaneously with the evolution of the electronic population. In Fig. 5(a), we show the Pearson correlation coefficients between the most varying internal coordinates and the valence-hole populations on N1, C5, C8, C9, O10, and water. It can be seen that the B(C5–C8) bond length, the θ(O9–C8–O10) angle, and the δ(N1–C5–H6–H7) dihedral angle are strongly correlated, and the change in the bond lengths B(C8–O9) and B(C9–O10) is strongly anticorrelated to the valence-hole population on the C5 atom of the $^{+}H_3NH_2C\cdot$. Remarkably, it turns out that this interdependence can be expressed through a linear combination of a few internal coordinates. Employing partial least squares regression (PLSR),[67] we identified a collective coordinate that explains 90% of the variance in the C5 hole population (R^2 = 0.90). A model with one component was used, meaning that predictor variables were condensed into a single variable to maximize covariance with the response. The time evolution along this linear coordinate is depicted in Fig. 5(b) along with the hole population on C5. This result suggests that the fragmentation reaction can be fully understood utilizing a one-dimensional reaction coordinate and that alternative reaction channels do not appear. The collective variation of glycine structural features along this reaction coordinate is depicted in Fig. 5(c). One can see how in the dissociation channel, the bonds B(C5–C8), B(C8–O9), and B(C9–O10) and the angles θ(O9–C8–O10) and δ(N1–C5–H6–H7) undergo a concerted movement.

D. Scenario B: Ionization of water

To consider ionization of water molecules in the vicinity of the glycine molecule, we focus on ionization in the wat-3a_1 MOs [see Fig. 2(a)]. For selecting the water MOs to ionize, we picked a random MO out of the identified wat-3a_1 orbitals, where a population threshold of 0.8 [somewhat tighter than in Fig. 2(a)] was used. This resulted in an ensemble of 51 trajectories. Initial ionization in the other water MOs reveals overall similar results but with slightly different electronic relaxation and fragmentation timings (not shown). The simulations were propagated for 200 fs, i.e., somewhat longer

than for scenario A, to account for the time it takes for the additional electronic relaxation. Our investigations focused on the processes taking place between water and glycine, such as the movement of the valence hole between these two regions. In particular, we observe how glycine is oxidized by ionized water.

Figure 6(a) shows the evolution of the valence-hole population on water molecules and on the glycine molecule, respectively. As can be seen, the valence hole that is initially entirely in water moves on a time scale of about 60 fs to the glycine moiety. This hole transfer is equivalent to the reduction of ionized water and the oxidation of glycine. By the end of the simulations, only a small hole population (0.06) remains in the water. Because in the situation considered in this section, ionization results in a considerably higher excited state than for scenario A, the movement of the valence hole is largely connected to electronic relaxation dynamics rather than geometrical changes. As the active state in the surface-hopping dynamics changes, the valence hole travels through the different MOs of the different moieties in the QM region.

Figure 6(b) shows the fraction of trajectories in the state with a hole in the HOMO, HOMO-1, and HOMO-2. As can be seen, at about 28.5 fs (dotted vertical line) after ionization, these states start to become populated, which coincides with the change in the valence-hole population in Fig. 6(a). Figure 6(b) also shows the fraction of trajectories that have dissociated along the C5–C8 bond. In this scenario, the fragmentation of glycine starts 93 fs after ionization, i.e., considerably delayed as compared to scenario A (see Fig. 4). This delay can be partially understood from the preceding electronic relaxation. Apart from this delay, we observe that in almost all trajectories, essentially the same dynamics occur as in scenario A: the glycine molecule eventually fragments into CO_2 and $^{+}H_3NH_2C\cdot$. The difference in the present scenario B is that the fragmentation is preceded by a redox reaction. The oxidizing agent is $H_2O\cdot^{+}$, which exists as a transient species in ionized water.[33,34,68] Our simulations illustrate the oxidizing power of $H_2O\cdot^{+}$ and its chemical implications.

In contrast to this major reaction channel, we observed two trajectories in which $H_2O\cdot^{+}$ turns into a hydroxyl radical (HO·) by transferring a proton to a neighboring water molecule. In those cases, the HO· radical formed does not react with glycine. Accordingly, the hole remains in water, explaining why the hole population

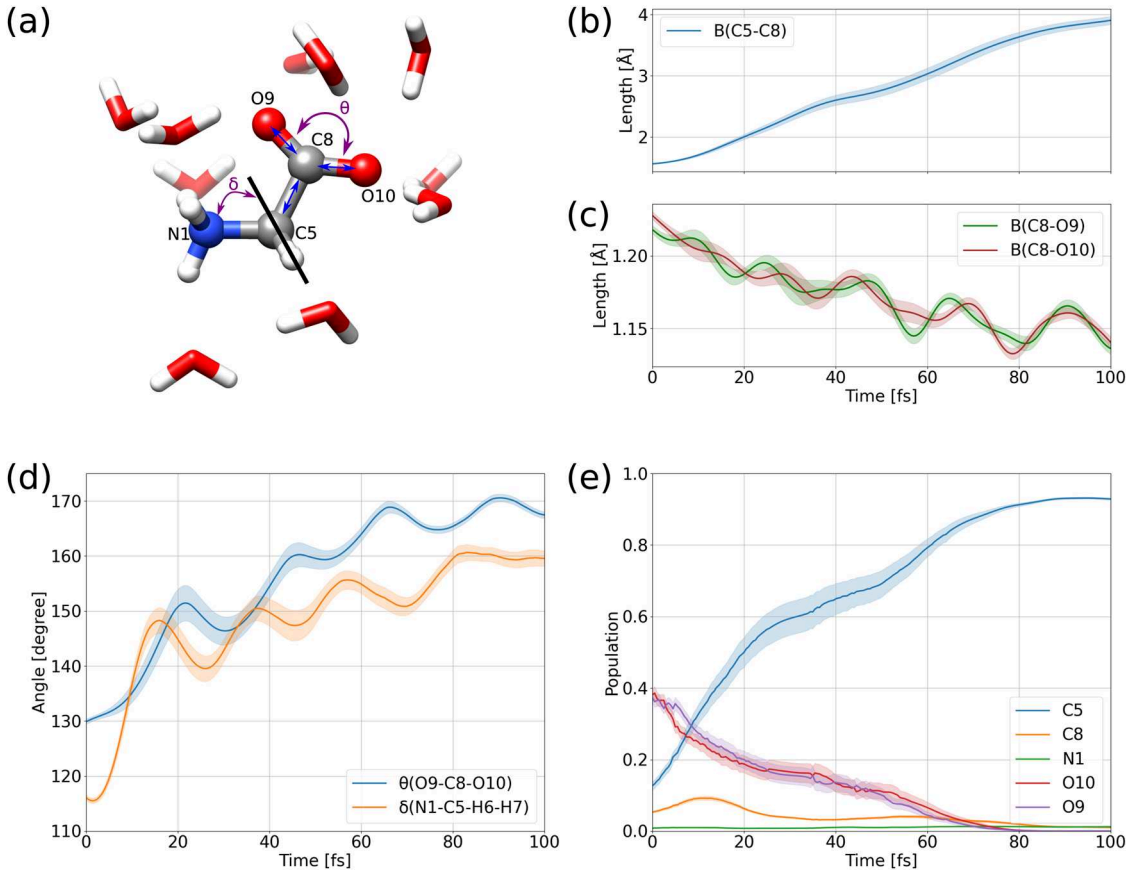

FIG. 4. Time evolution of internal coordinates for the 82 dissociating trajectories. (a) Glycine surrounded by ten water molecules, with atoms labeled in black (example from one initial geometry). The internal coordinates with the largest variance upon dissociation are represented: the bond lengths (blue arrows) B(C5–C8), B(C8–O9), and B(C8–O10); and the two angles (purple arrows) θ(O9–C8–O10) and δ(N1–C5–H6–H7). Time evolution for the dissociating trajectories of the B(C5–C8) bond length (b), the B(C8–O9) and B(C8–O10) bond lengths (c), the θ(O9–C8–O10) angle, and the δ(N1–C5–H6–H7) dihedral angle (d). Time evolution of valence-hole population on glycine atoms (e). Each curve shows the mean value. The shaded area depicts the standard error.

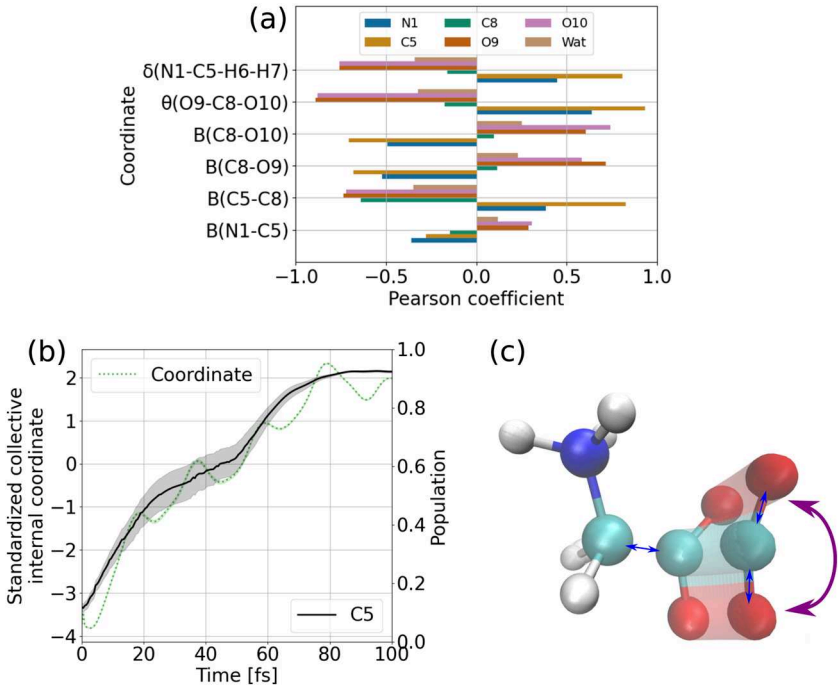

FIG. 5. Correlations between variables. (a) Pearson correlation coefficients between internal coordinates and electronic populations on N1, C5, C8, O9, O10, and water. (b) Left *y* axis: collective time variation of B(C5–C8), B(C8–O9), B(C8–O10), θ(O9–C8–O10), and δ(N1–C5–H6–H7) (green dotted line). Right *y* axis: time variation of the C5 electronic population (black solid line). Each curve shows the mean value with the standard error. (c) Identified collective coordinate.

of water is not zero at the end of the simulations [Fig. 6(a)]. This alternative reaction channel, water radiolysis, has previously been studied for pure water.[33,34,55] In the present study, owing to the limited size of the QM region, water radiolysis is artificially suppressed because the ionized water molecule cannot donate a proton to the surrounding water molecules in the MM region. This reaction channel would be much more abundant in a real aqueous solution of glycine, specifically for water molecules further from the vicinity of glycine. The created solvated proton and the HO· radical will diffuse through water and may subsequently react with glycine. However, since such processes occur on time scales controlled by diffusion, they lie outside the time window covered in this work.

E. Scenario C: Ionization of HOMO-41

In a third scenario, we inspected the ionization of glycine in its deeper bound valence orbital HOMO-41 (gly-9a′). Because of

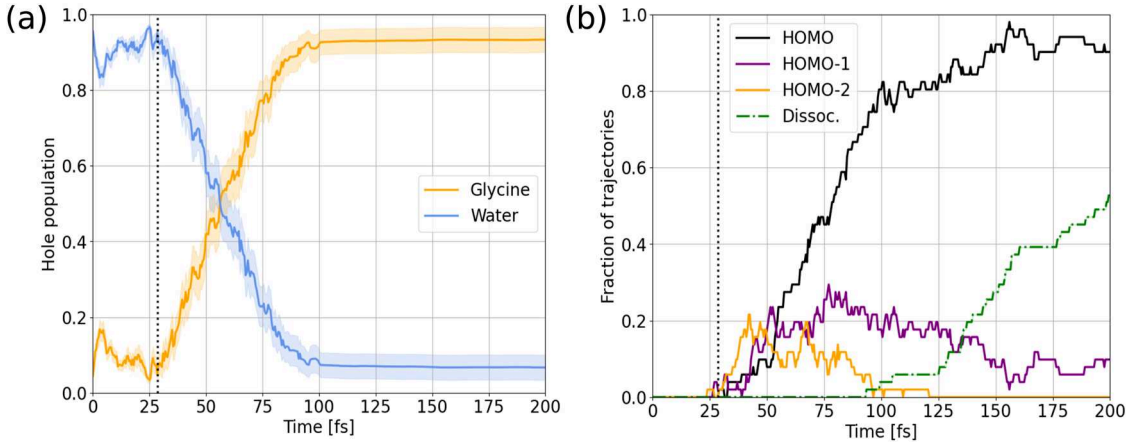

FIG. 6. Time evolution of the 51 trajectories after ionization of wat-3a_1. (a) Population of the hole in glycine (orange) or water (blue). The curves show the mean value with the standard error. (b) Fraction of trajectories relaxed to a state with a valence hole in the HOMO (black), HOMO-1 (purple), HOMO-2 (orange, solid lines), and fraction of trajectories in which glycine dissociation has taken place (green dashed-dotted line). The vertical dotted lines show the initiation of both valence-hole transfer from water to glycine (a) and relaxation of the system (b).

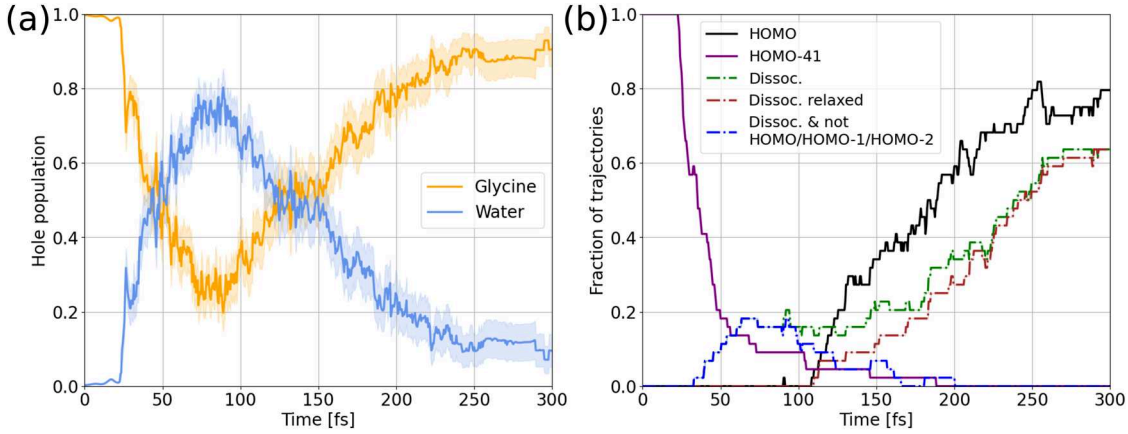

FIG. 7. Analysis of structural and electronic changes with time for initial ionization in HOMO-41 (44 trajectories). (a) Population of the valence hole on glycine (orange) or water (blue). Each curve shows the mean value with the standard error. (b) Fraction of trajectories in HOMO and HOMO-41–hole states (black/purple lines, respectively); fraction of dissociated trajectories (green dashed-dotted line); fraction of dissociated trajectories in an electronic state with a valence hole in the HOMO (brown, dashed-dotted line); and fraction of dissociated trajectories with a valence hole not in the HOMO, HOMO-1, or HOMO-2 (blue, dashed-dotted line).

the high electronic excitation, we need to consider a much longer cascade of electronic relaxations and, therefore, propagated the simulations up to 300 fs. In addition, the considerable energetic gap in the binding energies to higher-lying orbitals prevents immediate electronic relaxation. In this scenario, due to the high initial electronic excitation, a much higher amount of vibrational energy is ultimately transferred to the system. This can lead to problems for the simulation, since trajectories approach regions where the electronic-structure calculation fails. Due to that effect, 44 trajectories, instead of 51, are presented in the following statistical analysis, as some of them had to be discarded due to convergence issues.

The valence-hole populations on water and glycine are shown in Fig. 7(a). As can be seen, a sequence of two redox reactions occurs: first, glycine with a hole in HOMO-41, which has a high oxidizing power, oxidizes neutral water. This leads to an increase in the water hole population (i.e., in the population of oxidized water) about 80 fs after ionization. After the hole has been transferred to water and glycine has become neutral again, the $H_2O^{\cdot+}$ radical formed in water oxidizes glycine by removing an electron from its HOMO, HOMO-1, or HOMO-2. This second redox reaction causes the drop in the population of oxidized water—and the concomitant rise in the population of oxidized glycine—and is similar to the redox reaction observed in scenario B.

Figure 7(b) displays the fraction of trajectories in the HOMO-41–hole state and in the HOMO-hole GS. The fraction of trajectories in the electronic GS starts increasing after about 110 fs, and complete relaxation of all trajectories is not achieved by the end of the simulations. The system travels through a sequence of various PESs, including those corresponding to a valence hole located on water, similar to scenario B. As previously observed, the valence-hole transfer to glycine is concomitant with the electronic relaxation to the HOMO-hole state. Figure 7(b) additionally shows the fraction of trajectories with a dissociated C5–C8 bond. In contrast to what we observed in the other scenarios, we have here considerable fragmentation of the molecule even before the electronic relaxation is completed. Further analysis reveals that early-time fragmentation occurring at around 50 fs is associated with trajectories for which the relaxation from the initial HOMO-41 state to the GS occurs relatively late. Thus, the glycine molecule has some time to evolve on the HOMO-41 hole-state PES, which already triggers C5–C8 bond breaking [Fig. 7(b), blue dashed-dotted line]. Again, the tendency to weaken the bond can intuitively be understood from the bonding character of the HOMO-41 [see Fig. 2(b)]. The dissociation occurring at later times (starting after 110 fs) is associated with the HOMO PES, as confirmed by the green and brown dashed-dotted lines of Fig. 7(b), which nearly overlap.

Finally, similarly to scenario B, we observed water radiolysis in rare cases (4.5% of trajectories). This explains why the valence hole is not fully located on glycine and remains in a 90/10 glycine/water ratio [Fig. 7(a)] at the end of the simulations.

F. H-bond analysis and comparison with simulations without water

Considering the significance of H-bonds in living organisms, we investigated the effects of the post-ionization dynamics on their network.

Figure 8 shows the number of H-bonds between glycine and water as a function of time for scenarios A (initial hole in the glycine HOMO, HOMO-1, or HOMO-2) and B (initial hole in wat-3a_1).

In scenario A, the number of H-bonds between water and glycine drops rapidly from six to three during the first 25 fs before slowly stabilizing around two (red solid line). Scenario B results in a delayed decrease in the number of H-bonds between glycine and its environment (blue dashed-dotted line), dropping rapidly after 50 fs by about the same magnitude and stabilizing at about 100 fs. This time scale corresponds to the time identified for the hole to transfer from water to glycine [Fig. 6(a)]. The number of H-bonds among water molecules is not strongly affected by the ionization and stays almost constant (not shown).

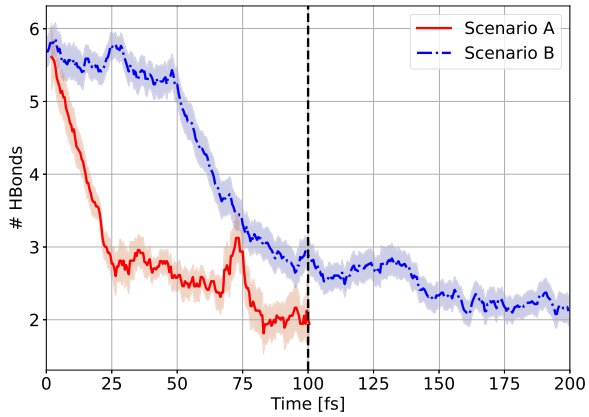

FIG. 8. Time evolution of the number of H-bonds between glycine and QM or MM water molecules in scenario A (red solid line) and scenario B (blue dashed-dotted line). The vertical dashed black line shows the end of the 100 fs simulations in scenario A. The curves display the mean value and the standard error (the latter in faded color).

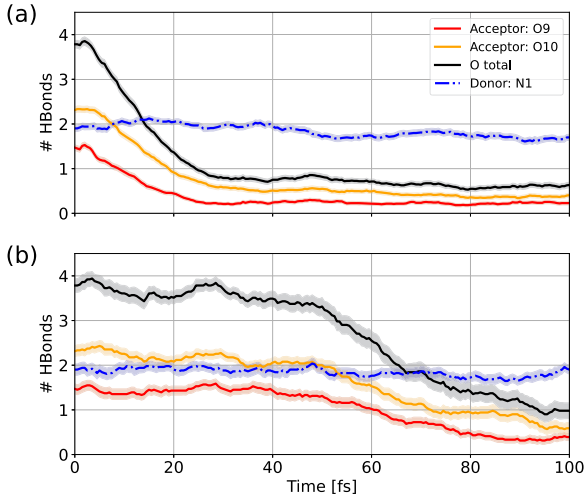

FIG. 9. Time evolution of the number of H-bonds between glycine and QM or MM water molecules. (a) Scenario A (glycine ionization in HOMO, HOMO-1, or HOMO-2). (b) Scenario B (wat-3a_1 ionization). H-bonds with O9 and O10 (red and orange solid lines), N1 (blue, dashed-dotted line), and the sum (black solid line) of the number of H-bonds with O9 and O10 are depicted. All curves show the mean value. Shaded areas indicate the standard error of the mean.

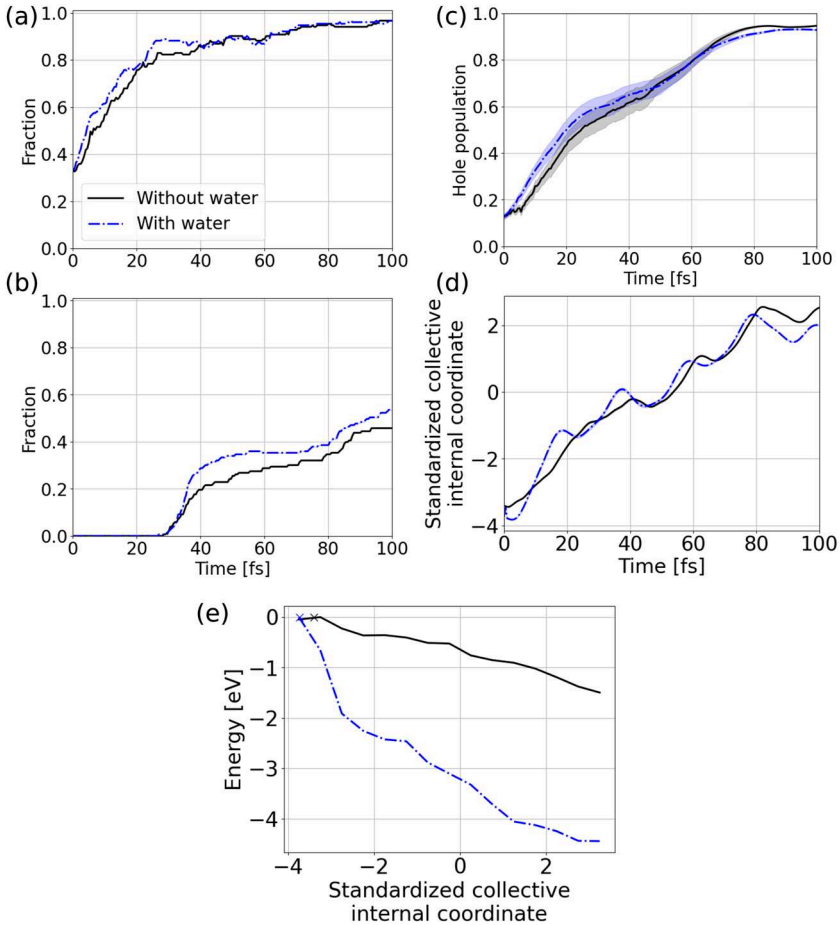

FIG. 10. Time evolution of various quantities along the dissociative trajectories with (83 trajectories, blue dashed-dotted line) and without (70 trajectories, black solid line) water. (a) Fraction of trajectories with the valence hole in the HOMO (relaxed). (b) Fraction of dissociated trajectories. (c) Valence-hole population on the C5 atom. (d) Collective coordinate obtained for simulations with (Fig. 5) (blue) and without water (black). (e) Potential energy along the collective coordinates obtained for simulations with (Fig. 5) (blue) and without water (black). Crosses represent the mean value at time 0.

Figure 9 shows the number of H-bonds between the O9, O10, and N1 glycine atoms and water in scenarios A and B, focusing on the first 100 fs. In both scenarios, the number of H-bonds with N1 remains close to two. In scenario A, the number of H-bonds with O9 and O10 significantly decreases within 30 fs, reaching a total value of about 0.6 (O9 and O10 summed together). This 30 fs time scale corresponds to the time glycine takes to dissociate in scenario A (see Fig. 3). The total number of H-bonds with O9 and O10 corresponds to the average number of H-bonds reported for solvated CO_2.[69]

In scenario B, the number of H-bonds with O9 and O10 remains almost constant around a value of four until it starts decreasing slowly after 30 fs, corresponding to the time required for the hole to be transferred to the glycine (see Fig. 6). Overall, we see that the major change in the H-bond structure occurs around the CO_2 moiety, whereas the number of H-bonds barely changes for the $^{+}H_3NH_2C\cdot$ moiety.

In addition to the influence of H-bonds, one might generally consider the possibility that the solvation shell influences the fragmentation of glycine. For instance, the chemical environment of the solvation shell would be expected to constrain the movement of the solute. In addition, the solvation shell has an influence on the shape of PESs and, thereby, can modulate reactivity. Therefore, in order to test the impact of the solvent on the dynamics, we performed a similar calculation as for scenario A but with the surrounding water molecules (from both the QM and MM regions) artificially removed. Without the solvation shell, one might expect that the fragmentation dynamics are accelerated, since the movement of the glycine molecule is less restricted. Figure 10 shows a comparative analysis of several features in the presence and absence of solvating water molecules, focusing only on the dissociating trajectories. In the absence of water, HOMO, HOMO-1, or HOMO-2 ionization leads to glycine fragmentation in 45.8% of the trajectories, which is slightly less than in aqueous conditions (53.0%). Electronic relaxation and dissociation are slightly delayed without water [Figs. 10(a) and 10(b)]. Similarly, the transfer of the valence hole to the C5 atom is slightly slower in the absence of water compared to the situation with water [Fig. 10(c)]. These results indicate that the whole process is actually slightly faster in the presence of the solvation shell.

In order to further compare the fragmentation dynamics, we calculated the collective coordinate with a PLSR fit for simulations of glycine without its solvation shell, as obtained in Fig. 5(b) for simulations with water. In Fig. 10(d), we compare the time evolution along this collective coordinate for both simulations. As can be seen, while the dynamics are slightly faster for the simulations with a solvation shell, the collective coordinate displays approximately the same temporal behavior in both simulations. In Fig. 10(e), we scan the potential energy along the collective coordinate in both simulations. To do so, we projected the trajectories on the collective coordinate and calculated the mean potential energy values within bins of 0.5 from the minimum to the maximum value of the collective coordinate. As can be seen, the decrease in the potential energy is much steeper in the presence of water, explaining why dissociation occurs slightly faster and in larger proportions.

IV. CONCLUSIONS

In summary, we have performed an extensive analysis of the dynamics following HOMO and deeper valence ionization of water-solvated glycine. Post-ionization *ab initio* nonadiabatic dynamics simulations were performed for the first time on this intricate system.

Upon ionization from one of the three orbitals with the lowest binding energy (HOMO, HOMO-1, and HOMO-2), glycine undergoes fragmentation on the C_α–C (C5–C8) bond, as previously reported in experimental and computational studies.[19,23,25–28] In addition, we shed light on the mechanisms giving rise to the formation of the products of the dissociation, CO_2 and $^{+}H_3NH_2C\cdot$. Based on the correlation with the hole population on the C5 atom, our analysis reveals that the fragmentation can be understood in terms of a single collective reaction coordinate.

Ionization of water orbitals is followed by electronic relaxation of the system to its GS, going hand in hand with oxidation of glycine by $H_2O\cdot^{+}$. In rare cases, water radiolysis can be seen, but in the majority of cases, ionizing a water molecule in the solvation shell leads to oxidation of glycine via internal-conversion mechanisms. A particularly intriguing situation arises when glycine is initially ionized in a more strongly bound orbital (HOMO-41). In that case, the resulting, electronically excited glycine cation acts as a strongly oxidizing agent that manages to oxidize water, thereby producing glycine in its neutral ground state. This first redox reaction is then followed by a second redox reaction associated with the oxidation of glycine by $H_2O\cdot^{+}$.

Finally, we show that the water–glycine H-bonds are not strongly affected by relaxation or valence-hole transfers. However, glycine dissociation alters the solvation shell, characterized by a different number of H-bonds connected to the CO_2 moiety. Comparison to simulations in which water was removed prior to ionization showed that the solvation shell slightly accelerates the dissociation.

We note that modeling highly excited states on the fly along molecular dynamics trajectories is a considerable challenge. The electronic-structure method employed here is restricted to the space of electronic one-hole configurations with respect to the Hartree–Fock ground-state reference. For higher excited states, the restriction to one-hole configurations becomes gradually more inaccurate, because mixing with two-hole–one-particle configurations becomes stronger. It certainly becomes problematic for inner-valence-hole states and core-level vacancies, for which substantial electronic many-body effects, including autoionization processes, are expected. At the same time, the method is highly robust since it only depends on the convergence of the Hartree–Fock procedure. Given the fact that the electronic relaxation occurs rather quickly, we think that the structural dynamics are captured semiquantitatively correctly. In light of the experimental observations,[19,23,25–28] the overall reaction routes given in our simulation model are also plausible. Nevertheless, a reliable electronic-structure method that can describe more intricate aspects of the electronic structure for a sufficiently large number of electronic states remains desirable. Combining such a method with FSSH simulations remains a challenge for the future.

Our results regarding the transfer of a valence hole from water to glycine, or from glycine to water, cast an interesting perspective on the radiation chemistry in aqueous solutions. Since water molecules typically outnumber the solute molecules by far, radiation damage is considered mainly an indirect effect. Primarily, water molecules are ionized, and the subsequently released pro-

tons and HO· radicals then react with the solvent molecule. In scenario B considered here, we highlight an entirely different mechanism: internal conversion can transport the valence hole to the solvent before water radiolysis takes place. At the same time, a valence hole can be created on the solute molecule and can then be transferred to water molecules in its solvation shell (scenario C). Such a mechanism is certainly limited to water molecules in the vicinity of the solute molecule. However, the exact limitations of this mechanism and how it competes with water radiolysis are still unclear and likely depend on characteristics of the solvent.

We envision that this mechanism for the sub-100 fs transfer of valence holes from water to a solvent molecule can be verified via ultrafast spectroscopy. An investigation on how the reported dynamics can be traced using time-dependent x-ray absorption spectroscopy will be the focus of future work.

SUPPLEMENTARY MATERIAL

The supplementary material includes analyses of radial distribution functions, collective coordination numbers, and potential-energy fluctuations for the FFMD and AIMD simulations.

ACKNOWLEDGMENTS

We thank Benoît Richard for the fruitful discussions. We acknowledge the support from DESY (Hamburg, Germany), a member of the Helmholtz Association (HGF). L.I. and R.S. further acknowledge the support from the Cluster of Excellence "CUI: Advanced Imaging of Matter" of the Deutsche Forschungsgemeinschaft (DFG)—EXC 2056—Project ID 390715994. The authors also acknowledge the scientific exchanges and support of the Center for Molecular Water Science (CMWS).

AUTHOR DECLARATIONS

Conflict of Interest

The authors have no conflicts to disclose.

Author Contributions

Mathilde Goullieux: Conceptualization (equal); Data curation (lead); Formal analysis (lead); Investigation (lead); Methodology (equal); Software (equal); Validation (equal); Visualization (equal); Writing – original draft (lead); Writing – review & editing (equal). **Anthony Ferté**: Conceptualization (equal); Methodology (equal); Supervision (supporting); Validation (equal); Visualization (equal); Writing – review & editing (equal). **Ana Martinez Gutierrez**: Conceptualization (equal); Formal analysis (supporting); Writing – review & editing (equal). **Ludger Inhester**: Conceptualization (equal); Funding acquisition (equal); Methodology (equal); Project administration (equal); Software (equal); Supervision (equal); Validation (equal); Visualization (equal); Writing – review & editing (lead). **Robin Santra**: Conceptualization (lead); Funding acquisition (lead); Methodology (equal); Project administration (lead); Resources (lead); Supervision (lead); Writing – review & editing (equal).

DATA AVAILABILITY

The data that support the findings of this study are available from the corresponding author upon reasonable request.

REFERENCES

[1] J. R. Cronin and S. Pizzarello, "Amino acids in meteorites," Adv. Space Res. **3**, 5–18 (1983).
[2] J. E. Elsila, D. P. Glavin, and J. P. Dworkin, "Cometary glycine detected in samples returned by stardust," Meteorit. Planet. Sci. **44**, 1323–1330 (2009).
[3] J. E. Elsila, J. C. Aponte, D. G. Blackmond, A. S. Burton, J. P. Dworkin, and D. P. Glavin, "Meteoritic amino acids: Diversity in compositions reflects parent body histories," ACS Cent. Sci. **2**, 370–379 (2016).
[4] K. Altwegg, H. Balsiger, A. Bar-Nun, J.-J. Berthelier, A. Bieler, P. Bochsler, C. Briois, U. Calmonte, M. R. Combi, H. Cottin, J. D. Keyser, F. Dhooghe, B. Fiethe, S. A. Fuselier, S. Gasc, T. I. Gombosi, K. C. Hansen, M. Haessig, A. Jäckel, E. Kopp, A. Korth, L. L. Roy, U. Mall, B. Marty, O. Mousis, T. Owen, H. Rème, M. Rubin, T. Sémon, C.-Y. Tzou, J. H. Waite, and P. Wurz, "Prebiotic chemicals-amino acid and phosphorus-in the coma of comet 67P/Churyumov-Gerasimenko," Sci. Adv. **2**, e1600285 (2016).
[5] D. P. Glavin, J. P. Dworkin, C. M. O. Alexander, J. C. Aponte, A. A. Baczynski, J. J. Barnes, H. A. Bechtel, E. L. Berger, A. S. Burton, P. Caselli, A. H. Chung, S. J. Clemett, G. D. Cody, G. Dominguez, J. E. Elsila, K. K. Farnsworth, D. I. Foustoukos, K. H. Freeman, Y. Furukawa, Z. Gainsforth, H. V. Graham, T. Grassi, B. M. Giuliano, V. E. Hamilton, P. Haenecour, P. R. Heck, A. E. Hofmann, C. H. House, Y. Huang, H. H. Kaplan, L. P. Keller, B. Kim, T. Koga, M. Liss, H. L. McLain, M. A. Marcus, M. Matney, T. J. McCoy, O. M. McIntosh, A. Mojarro, H. Naraoka, A. N. Nguyen, M. Nuevo, J. A. Nuth, Y. Oba, E. T. Parker, T. S. Peretyazhko, S. A. Sandford, E. Santos, P. Schmitt-Kopplin, F. Seguin, D. N. Simkus, A. Shahid, Y. Takano, K. L. Thomas-Keprta, H. Tripathi, G. Weiss, Y. Zheng, N. G. Lunning, K. Righter, H. C. Connolly, and D. S. Lauretta, "Abundant ammonia and nitrogen-rich soluble organic matter in samples from asteroid (101955) Bennu," Nat. Astron. **9**, 199–210 (2025).
[6] G. M. Muñoz Caro, U. J. Meierhenrich, W. A. Schutte, B. Barbier, A. Arcones Segovia, H. Rosenbauer, W. H.-P. Thiemann, A. Brack, and J. M. Greenberg, "Amino acids from ultraviolet irradiation of interstellar ice analogues," Nature **416**, 403–406 (2002).
[7] R. L. Hudson, M. H. Moore, J. P. Dworkin, M. P. Martin, and Z. D. Pozun, "Amino acids from ion-irradiated nitrile-containing ices," Astrobiology **8**, 771–779 (2008).
[8] P. A. Gerakines and R. L. Hudson, "Glycine's radiolytic destruction in ices: First *in situ* laboratory measurements for Mars," Astrobiology **13**, 647–655 (2013).
[9] A. Pernet, J. Pilmé, F. Pauzat, Y. Ellinger, F. Sirotti, M. Silly, Ph. Parent, and C. Laffon, "Possible survival of simple amino acids to X-ray irradiation in ice: The case of glycine," A&A **552**, A100 (2013).
[10] Z. Yin, Y.-P. Chang, T. Balčiūnas, Y. Shakya, A. Djorović, G. Gaulier, G. Fazio, R. Santra, L. Inhester, J.-P. Wolf, and H. J. Wörner, "Femtosecond proton transfer in urea solutions probed by X-ray spectroscopy," Nature **619**, 749–754 (2023).
[11] K. Ohnishi and T. Ohnishi, "The biological effects of space radiation during long stays in space," Biol. Sci. Space **18**, 201–205 (2004).
[12] A. A. Voorhies, C. M. Ott, S. Mehta *et al.*, "Study of the impact of long-duration space missions at the international space station on the astronaut microbiome," Sci. Rep. **9**, 9911 (2019).
[13] National Academies of Sciences, Engineering, and Medicine, "Space radiation and cancer risks to astronauts," in *Space Radiation and Astronaut Health: Managing and Communicating Cancer Risks* (The National Academies Press, Washington DC, 2021), Chap. 2, p. 33.
[14] G. Minniti, C. Goldsmith, and M. Brada, "Chapter 16—Radiotherapy," in *Handbook of Clinical Neurology: Neuro-Oncology*, edited by M. J. Aminoff, F. Boller, and D. F. Swaab (Elsevier, 2012), Vol. 104, pp. 215–228.
[15] B. C. Garrett, D. A. Dixon, D. M. Camaioni, D. M. Chipman, M. A. Johnson, C. D. Jonah, G. A. Kimmel, J. H. Miller, T. N. Rescigno, P. J. Rossky, S. S. Xantheas, S. D. Colson, A. H. Laufer, D. Ray, P. F. Barbara, D. M. Bartels, K. H. Becker, K. H. Bowen, Jr., S. E. Bradforth, I. Carmichael, J. V. Coe, L. R. Corrales, J. P. Cowin, M. Dupuis, K. B. Eisenthal, J. A. Franz, M. S. Gutowski, K. D. Jordan,

B. D. Kay, J. A. LaVerne, S. V. Lymar, T. E. Madey, C. W. McCurdy, D. Meisel, S. Mukamel, A. R. Nilsson, T. M. Orlando, N. G. Petrik, S. M. Pimblott, J. R. Rustad, G. K. Schenter, S. J. Singer, A. Tokmakoff, L.-S. Wang, and T. S. Zwier, "Role of water in electron-initiated processes and radical chemistry: Issues and scientific advances," Chem. Rev. **105**, 355–390 (2005).
[16]A. D. Buckingham, J. E. Del Bene, and S. A. C. McDowell, "The hydrogen bond," Chem. Phys. Lett. **463**, 1–10 (2008).
[17]L. J. Karas, C.-H. Wu, R. Das, and J. I.-C. Wu, "Hydrogen bond design principles," Wiley Interdiscip. Rev.: Comput. Mol. Sci. **10**, e1477 (2020).
[18]R. Tripathi, L. Durán Caballero, R. Pérez de Tudela, C. Hölzl, and D. Marx, "Unveiling zwitterionization of glycine in the microhydration limit," ACS Omega **6**, 12676–12683 (2021).
[19]H.-W. Jochims, M. Schwell, J.-L. Chotin, M. Clemino, F. Dulieu, H. Baumgärtel, and S. Leach, "Photoion mass spectrometry of five amino acids in the 6–22 eV photon energy range," Chem. Phys. **298**, 279–297 (2004).
[20]A. F. Lago, L. H. Coutinho, R. R. T. Marinho, A. Naves de Brito, and G. G. B. de Souza, "Ionic dissociation of glycine, alanine, valine and proline as induced by VUV (21.21 eV) photons," Chem. Phys. **307**, 9–14 (2004).
[21]M. C. Castrovilli, A. Trabattoni, P. Bolognesi, P. O'Keeffe, L. Avaldi, M. Nisoli, F. Calegari, and R. Cireasa, "Ultrafast hydrogen migration in photoionized glycine," J. Phys. Chem. Lett. **9**, 6012–6016 (2018).
[22]J. Chiarinelli, P. Bolognesi, A. Domaracka, P. Rousseau, M. C. Castrovilli, R. Richter, S. Chatterjee, F. Wang, and L. Avaldi, "Insights into the dissociative ionization of glycine by PEPICO experiments," Phys. Chem. Chem. Phys. **20**, 22841–22848 (2018).
[23]E. Itälä, K. Kooser, E. Rachlew, M. A. Huels, and E. Kukk, "Soft x-ray ionization induced fragmentation of glycine," J. Chem. Phys. **140**, 234305 (2014).
[24]D. Schwickert, M. Ruberti, P. Kolorenč, S. Usenko, A. Przystawik, K. Baev, I. Baev, M. Braune, L. Bocklage, M. K. Czwalinna, S. Deinert, S. Düsterer, A. Hans, G. Hartmann, C. Haunhorst, M. Kuhlmann, S. Palutke, R. Röhlsberger, J. Rönsch-Schulenburg, P. Schmidt, S. Toleikis, J. Viefhaus, M. Martins, A. Knie, D. Kip, V. Averbukh, J. P. Marangos, and T. Laarmann, "Electronic quantum coherence in glycine molecules probed with ultrashort x-ray pulses in real time," Sci. Adv. **8**, eabn6848 (2022).
[25]S. Maclot, M. Capron, R. Maisonny, A. Ławicki, A. Méry, J. Rangama, J.-Y. Chesnel, S. Bari, R. Hoekstra, T. Schlathölter, B. Manil, L. Adoui, P. Rousseau, and B. A. Huber, "Ion-induced fragmentation of amino acids: Effect of the environment," ChemPhysChem **12**, 930–936 (2011).
[26]S. Nomura, H. Tsuchida, R. Furuya, T. Majima, and A. Itoh, "Fast heavy-ion radiation damage of glycine in aqueous solution," Nucl. Instrum. Methods Phys. Res., Sect. B **389-390**, 28–32 (2016).
[27]D. Shemesh, G. M. Chaban, and R. B. Gerber, "Photoionization dynamics of glycine: The first 10 picoseconds," J. Phys. Chem. A **108**, 11477–11484 (2004).
[28]R. G. Wilks, J. B. MacNaughton, H.-B. Kraatz, T. Regier, R. I. R. Blyth, and A. Moewes, "Comparative theoretical and experimental study of the radiation-induced decomposition of glycine," J. Phys. Chem. A **113**, 5360–5366 (2009).
[29]Z. Li, M. El-Amine Madjet, O. Vendrell, and R. Santra, "Core-level transient absorption spectroscopy as a probe of electron hole relaxation in photoionized $H^+(H_2O)_n$," Faraday Discuss. **171**, 457–470 (2014).
[30]J. C. Tully, "Molecular dynamics with electronic transitions," J. Chem. Phys. **93**, 1061–1071 (1990).
[31]K. Khalili, L. Inhester, C. Arnold, R. Welsch, J. W. Andreasen, and R. Santra, "Hole dynamics in a photovoltaic donor-acceptor couple revealed by simulated time-resolved X-ray absorption spectroscopy," Struct. Dyn. **6**, 044102 (2019).
[32]K. Khalili, L. Inhester, C. Arnold, A. S. Gertsen, J. W. Andreasen, and R. Santra, "Simulation of time-resolved x-ray absorption spectroscopy of ultrafast dynamics in particle-hole-excited 4-(2-thienyl)-2,1,3-benzothiadiazole," Struct. Dyn. **7**, 044101 (2020).
[33]Z.-H. Loh, G. Doumy, C. Arnold, L. Kjellsson, S. H. Southworth, A. A. Haddad, Y. Kumagai, M.-F. Tu, P. J. Ho, A. M. March, R. D. Schaller, M. S. B. M. Yusof, T. Debnath, M. Simon, R. Welsch, L. Inhester, K. Khalili, K. Nanda, A. I. Krylov, S. Moeller, G. Coslovich, J. Koralek, M. P. Minitti, W. F. Schlotter, J.-E. Rubensson, R. Santra, and L. Young, "Observation of the fastest chemical processes in the radiolysis of water," Science **367**, 179–182 (2020).
[34]L. Inhester, A. S. Moros, S. Macé, C. Arnold, and R. Santra, "Ionization-induced proton and energy transfer in liquid water," J. Chem. Phys. **162**, 154503 (2025).
[35]Y. Shakya, L. Inhester, C. Arnold, R. Welsch, and R. Santra, "Ultrafast time-resolved x-ray absorption spectroscopy of ionized urea and its dimer through *ab initio* nonadiabatic dynamics," Struct. Dyn. **8**, 034102 (2021).
[36]wwPDB Consortium, "Protein Data Bank: The single global archive for 3D macromolecular structure data," Nucleic Acids Res. **47**, D520–D528 (2018).
[37]N. M. O'Boyle, M. Banck, C. A. James, C. Morley, T. Vandermeersch, and G. R. Hutchison, "Open Babel: An open chemical toolbox," J. Cheminform. **3**, 33 (2011).
[38]Open Babel v2.3.2, http://openbabel.org (2012); accessed October 2012.
[39]H. Miyamoto and M. Aida, "Helmholtz energy change between neutral and zwitterionic forms of glycine in aqueous solution using *ab initio* expanded QM/MM-MC with QM solvent," Chem. Lett. **42**, 1010–1012 (2013).
[40]R. Boča, J. Štofko, and R. Imrich, "Effect of solvation on glycine molecules: A theoretical study," ACS Omega **8**, 28577–28582 (2023).
[41]M. J. Abraham, T. Murtola, R. Schulz, S. Páll, J. C. Smith, B. Hess, and E. Lindahl, "GROMACS: High performance molecular simulations through multi-level parallelism from laptops to supercomputers," SoftwareX **1-2**, 19–25 (2015).
[42]H. J. C. Berendsen, J. P. M. Postma, W. F. van Gunsteren, A. DiNola, and J. R. Haak, "Molecular dynamics with coupling to an external bath," J. Chem. Phys. **81**, 3684–3690 (1984).
[43]A. D. MacKerell, Jr., D. Bashford, M. Bellott, R. L. Dunbrack, J. D. Evanseck, M. J. Field, S. Fischer, J. Gao, H. Guo, S. Ha, D. Joseph-McCarthy, L. Kuchnir, K. Kuczera, F. T. K. Lau, C. Mattos, S. Michnick, T. Ngo, D. T. Nguyen, B. Prodhom, W. E. Reiher, B. Roux, M. Schlenkrich, J. C. Smith, R. Stote, J. Straub, M. Watanabe, J. Wiórkiewicz-Kuczera, D. Yin, and M. Karplus, "All-atom empirical potential for molecular modeling and dynamics studies of proteins," J. Phys. Chem. B **102**, 3586–3616 (1998).
[44]A. D. Mackerell, Jr., M. Feig, and C. L. Brooks III, "Extending the treatment of backbone energetics in protein force fields: Limitations of gas-phase quantum mechanics in reproducing protein conformational distributions in molecular dynamics simulations," J. Comput. Chem. **25**, 1400–1415 (2004).
[45]P. Bjelkmar, P. Larsson, M. A. Cuendet, B. Hess, and E. Lindahl, "Implementation of the CHARMM force field in GROMACS: Analysis of protein stability effects from correction maps, virtual interaction sites, and water models," J. Chem. Theory Comput. **6**, 459–466 (2010).
[46]W. L. Jorgensen, J. Chandrasekhar, J. D. Madura, R. W. Impey, and M. L. Klein, "Comparison of simple potential functions for simulating liquid water," J. Chem. Phys. **79**, 926–935 (1983).
[47]E. Neria, S. Fischer, and M. Karplus, "Simulation of activation free energies in molecular systems," J. Chem. Phys. **105**, 1902–1921 (1996).
[48]G. Alagona, C. Ghio, and P. A. Kollman, "Monte Carlo simulation studies of the solvation of ions. 2. Glycine zwitterion," J. Mol. Struct.: THEOCHEM **166**, 385–392 (1988), part of Special Issue: Proceedings of the XVIIth International Congress of Theoretical Chemists of Latin Expression.
[49]S. Gnanasambandam, Z. Hu, J. Jiang, and R. Rajagopalan, "Force field for molecular dynamics studies of glycine/water mixtures in crystal/solution environments," J. Phys. Chem. B **113**, 752–758 (2009).
[50]K. Leung and S. B. Rempe, "*Ab initio* molecular dynamics study of glycine intramolecular proton transfer in water," J. Chem. Phys. **122**, 184506 (2005).
[51]M. G. Campo, "Molecular dynamics simulation of glycine zwitterion in aqueous solution," J. Chem. Phys. **125**, 114511 (2006).
[52]J. Sun, D. Bousquet, H. Forbert, and D. Marx, "Glycine in aqueous solution: Solvation shells, interfacial water, and vibrational spectroscopy from *ab initio* molecular dynamics," J. Chem. Phys. **133**, 114508 (2010).
[53]L. Inhester, K. Hanasaki, S.-K. Son, Y. Hao, C. Arnold, K. Khalili, A. Sopena, A. Ferté, and R. Santra, "XMOLECULE—Molecular electronic structure for X-ray physics," XRAYPAC, Version 2.1.0, GitLab, https://gitlab.desy.de/CDT/xraypac, 2025.
[54]Y. Hao, L. Inhester, K. Hanasaki, S.-K. Son, and R. Santra, "Efficient electronic structure calculation for molecular ionization dynamics at high x-ray intensity," Struct. Dyn. **2**, 041707 (2015).
[55]L. Inhester, K. Hanasaki, Y. Hao, S.-K. Son, and R. Santra, "X-ray multiphoton ionization dynamics of a water molecule irradiated by an x-ray free-electron laser pulse," Phys. Rev. A **94**, 023422 (2016).
[56]W. J. Hehre, R. Ditchfield, and J. A. Pople, "Self-consistent molecular orbital methods. XII. Further extensions of Gaussian-type basis sets for use in molecular orbital studies of organic molecules," J. Chem. Phys. **56**, 2257–2261 (1972).

[57]P. C. Hariharan and J. A. Pople, "The influence of polarization functions on molecular orbital hydrogenation energies," Theor. Chim. Acta **28**, 213–222 (1973).
[58]B. Cordero, V. Gómez, A. E. Platero-Prats, M. Revés, J. Echeverría, E. Cremades, F. Barragán, and S. Alvarez, "Covalent radii revisited," Dalton Trans. **21**, 2832–2838 (2008).
[59]N. Michaud-Agrawal, E. J. Denning, T. B. Woolf, and O. Beckstein, "MDAnalysis: A toolkit for the analysis of molecular dynamics simulations," J. Comput. Chem. **32**, 2319–2327 (2011).
[60]R. J. Gowers, M. Linke, J. Barnoud, T. J. E. Reddy, M. N. Melo, S. L. Seyler, J. Domański, D. L. Dotson, S. Buchoux, I. M. Kenney, and O. Beckstein, "MDAnalysis: A Python package for the rapid analysis of molecular dynamics simulations," in *Proceedings of the 15th Python in Science Conference*, edited by S. Benthall and S. Rostrup (SciPy, 2016), pp. 98–105.
[61]A. Sopena Moros, S. Li, K. Li, G. Doumy, S. H. Southworth, C. Otolski, R. D. Schaller, Y. Kumagai, J.-E. Rubensson, M. Simon, G. Dakovski, K. Kunnus, J. S. Robinson, C. Y. Hampton, D. J. Hoffman, J. Koralek, Z.-H. Loh, R. Santra, L. Inhester, and L. Young, "Tracking cavity formation in electron solvation: Insights from X-ray spectroscopy and theory," J. Am. Chem. Soc. **146**, 3262–3269 (2024).
[62]C. T. Falzon and F. Wang, "Understanding glycine conformation through molecular orbitals," J. Chem. Phys. **123**, 214307 (2005).
[63]A. Üngördü and N. Tezer, "The solvent (water) and metal effects on HOMO-LUMO gaps of guanine base pair: A computational study," J. Mol. Graph. **74**, 265–272 (2017).
[64]Jmol Development Team, "Jmol: An open-source Java viewer for chemical structures in 3D," http://www.jmol.org/, 2025; accessed 28 October 2025.
[65]G. Herzberg, *Electronic Spectra and Electronic Structure of Polyatomic Molecules* (Van Nostrand, New York, 1966).
[66]D. A. Armstrong, A. Rauk, and D. Yu, "Aminoalkyl and alkylaminium free radicals and related species: Structures, thermodynamic properties, reduction potentials, and aqueous free energies," J. Am. Chem. Soc. **115**, 666–673 (1993).
[67]S. Wold, M. Sjöström, and L. Eriksson, "PLS-regression: A basic tool of chemometrics," Chemom. Intell. Lab. Syst. **58**, 109–130 (2001), part of Special Issue: PLS Methods.
[68]J. Ma, F. Wang, and M. Mostafavi, "Ultrafast chemistry of water radical cation, $H_2O^{\cdot+}$, in aqueous solutions," Molecules **23**, 244 (2018).
[69]R. K. Lam, A. H. England, J. W. Smith, A. M. Rizzuto, O. Shih, D. Prendergast, and R. J. Saykally, "The hydration structure of dissolved carbon dioxide from X-ray absorption spectroscopy," Chem. Phys. Lett. **633**, 214–217 (2015).